International Journal of Mass Spectrometry 283 (2009) 112–121

Contents lists available at ScienceDirect

International Journal of Mass Spectrometry

journal homepage: www.elsevier.com/locate/ijms

HCN detection with a proton transfer reaction mass spectrometer

W.B. Knighton[a,*], E.C. Fortner[a], Anthony J. Midey[b,c], A.A. Viggiano[b], S.C. Herndon[d], E.C. Wood[d], C.E. Kolb[d]

[a] Department of Chemistry and Biochemistry, Montana State University, Bozeman, MT 59717, United States
[b] Air Force Research Laboratory, Space Vehicles Directorate, 29 Randolph Road, Hanscom AFB, MA 01731-3010, United States
[c] Institute for Scientific Research, Boston College, Chestnut Hill, MA, United States
[d] Aerodyne Research Inc., 45 Manning Road, Billerica, MA 01821-3976, United States

ARTICLE INFO

Article history:
Received 1 December 2008
Received in revised form 11 February 2009
Accepted 13 February 2009
Available online 24 February 2009

Keywords:
HCN
PTR-MS
SIFT
Proton transfer
Chemical ionization

ABSTRACT

Proton transfer reaction mass spectrometry (PTR-MS) is a promising technique for making rapid, sensitive measurements of HCN in the atmosphere. However, because the proton affinity of HCN is only slightly greater than that of water, the reverse proton transfer reaction of protonated HCN with water is important and the PTR-MS response to HCN is temperature and humidity dependent. The instrument response of a PTR-MS was calibrated at a variety of HCN mixing ratios, temperatures and relative humidities. A simple model with a kinetic and thermodynamic basis was developed to fit these results and accurately accounted for the temperature and humidity dependence of these measurements. Reaction rate coefficients were determined using a selected ion flow tube mass spectrometer (SIFT). Changes in sensitivity due to variations in temperature and humidity were simply and accurately corrected for using measurable parameters, including the $H_3O^+(H_2O)$ to H_3O^+ ratio as a measure of the water vapor concentration along with an empirically determined temperature and pressure correction factor. This calibration procedure should be applicable to the quantification of other compounds possessing proton affinities similar to that of HCN such as formaldehyde and hydrogen sulfide. The technique was applied during a two-week ambient measurement period. Analysis of that data suggests that ethene is a spectral interferent. The ethene interference arises due to the presence of O_2^+, which is generated as an unwanted byproduct as a result of using a low-pressure hollow cathode discharge as an external ion source. O_2^+ reacts with ethene via charge transfer reaction to form $C_2H_4^+$, which has the same mass-to-charge ratio as protonated HCN. The magnitude of the ethene interference is estimated at 0.1 ppbv HCN equivalent per ppbv of ethene. The ethene interference can be controlled through reducing or eliminating the amount of O_2^+. HCN concentrations deduced from the ambient measurements after correction for the ethene interference appear reasonable and provide evidence that PTR-MS instruments can be employed for the measurement of HCN.

1. Introduction

Hydrogen cyanide (HCN) is an important atmospheric tracer compound usually associated with biomass burning [1]. While it is generally accepted from a global perspective that biomass burning is a dominant source of HCN, biogenic and urban/industrial sources also have significant contributions [2]. Several studies have now identified vehicle exhaust as an emission source of HCN [3,4]. Because biomass burning tracers play an important role in quantifying the influence that fires have on local and regional air quality there is a clear need for sensitive methods that can interrogate and distinguish these biomass emissions from urban/industrial and vehicular sources.

Chemical ionization mass spectrometry (CIMS) has become a valuable tool for the real-time, on-line analysis of a variety of trace gases in challenging matrices such as human breath, engine exhaust, wildfire plumes, polluted and ambient atmospheres. A number of different CIMS techniques have been applied to the analysis of HCN. Carbonate ion CIMS has demonstrated some of the highest reported detection sensitivities and has been successfully used for the in-situ measurement of HCN in the relatively dry regions of the upper troposphere and the lower stratosphere [5,6]. In the lower troposphere, clustering reactions of the carbonate ion with ambient water reduce the utility of this method. The hydroxide ion (OH^-) has been used to detect HCN emitted from wounded clover via a proton abstraction reaction utilizing a selected ion flow tube mass spectrometer (SIFT) [7]. Given the large reaction rate constant for the reaction of HCN with OH^- [8], and the lack of any isobaric interferences OH^- CIMS represents an attractive method for the detection HCN. Positive ion CIMS using H_3O^+ as a reagent

* Corresponding author. Tel.: +1 406 994 5419; fax: +1 406 994 5407.
E-mail address: bknighton@chemistry.montana.edu (W.B. Knighton).

1387-3806/$ – see front matter © 2009 Elsevier B.V. All rights reserved.
doi:10.1016/j.ijms.2009.02.013

ion has been applied to the detection of HCN in SIFT [9] and proton transfer reaction mass spectrometers (PTR-MS) [10–13]. All of these reports indicate that accurate quantification of HCN via proton transfer with H_3O^+ is difficult due to the reverse reaction of protonated HCN with water since the proton affinity of HCN is only slightly greater than that of water. Because PTR-MS instruments are often used to measure volatile organic compounds in ambient and polluted atmospheres [14] where concurrent measurement of HCN would be useful, we have examined the feasibility of extracting quantitative information on HCN using the PTR-MS technique.

The difficulty of using proton transfer for the detection of HCN is well recognized [9–13]. Because the proton affinity (PA) of HCN (PA = 712.9 kJ mol^{-1}) [15] is slightly greater that that of water (PA = 691 kJ mol^{-1}) [15] and the H_2O concentrations greatly exceed those of HCN, the detection efficiency is significantly influenced by the reverse reaction of protonated HCN with water. The detection and quantification of formaldehyde (PA = 712.9 kJ mol^{-1}) [15], which has the same proton affinity, is also affected by the influence of water and has been discussed by numerous authors [13,16–19]. Since the quantification of HCN and formaldehyde are similarly influenced by the presence of water, the following literature review includes work done on both systems. Hansel et al. [16] studied the energy dependence of the proton transfer reactions of H_3O^+ with HCHO and $HCHOH^+$ with H_2O. Based on the reaction kinetics defined in that study, one expects the observed PTR-MS response to HCHO or HCN to be reduced by about a factor of 4 at 50% relative humidity and room temperature. This result has generally been corroborated in subsequent studies. In a laboratory inter-comparison with a Hantzsch instrument, Steinbacher et al. [18] observed that the PTR-MS response of formaldehyde was reduced by a factor of 4.8 in a calibration experiment using dry air and a permeation source. However, in that same study the PTR-MS surprisingly showed an improved response when measuring higher humidity laboratory air where the response was only a factor of 2.6 lower than that measured by the Hantzsch monitor. Christian et al. [10] in an inter-comparison study of biomass burning emissions found that the PTR-MS response to HCHO was a factor of 3 lower and HCN a factor of 12 lower than the measurements provided by a Fourier transform infrared (FTIR) spectrometer. In a follow up study [13] in controlled laboratory burns (~50% relative humidity), it was observed that the PTR-MS response to HCN was consistently about a factor of 5 lower than the FTIR value. A comparison of the field data collected for HCHO exhibited a strong humidity dependence in which the PTR-MS response, as compared to the FTIR, was more wide-ranging and varied from a factor of 5 lower at the lowest humidity to a factor of 20 times lower at the highest humidities. Modeling studies of that data suggested the presence of more water in the drift tube than could be attributed to sample humidity alone. From this result, the authors inferred that a significant amount of water from the hollow cathode ion source was leaking into the drift tube and suggested using the intensity of the $H_3O^+(H_2O)$ ion as relative measure of the total water vapor level. The influence of water entering the PTR-MS drift tube from the hollow cathode ion source has been previously noted and characterized [20]. An important consequence of that study by Amman et al. was the demonstration that the $H_3O^+(H_2O)$ ion intensity was a stable measure of water vapor concentration within the drift tube and that after suitable calibration the proton hydrate ion intensities could be used to deduce the concentration of water in ambient samples. More recently, Inomata et al. [17] calibrated their PTR-MS response to HCHO as a function of sample humidity and derived a calibration factor that independently accounted for the contributions of water vapor coming from the hollow cathode ion source and the ambient sample. HCHO concentrations deduced from their humidity corrected calibration response factors were found to be in excellent agreement with measurements made by multi-axis differential optical absorption spectroscopy (MAX-DOAS).

In all of the studies discussed above, the PTR-MS responses were calibrated with respect to the ambient humidity of the sample. While this is a logical approach it necessitates an independent measure of the humidity of the ambient sample and still requires an independent assessment of the water introduced from the hollow cathode ion source. In this study, we demonstrate a method to calibrate the response of a PTR-MS to HCN using the measured H_3O^+ and $H_3O^+(H_2O)$ ion signals to compensate for any changes in the HCN detection efficiency with humidity. A consequence of using the H_3O^+ and $H_3O^+(H_2O)$ ion distribution to provide an accurate measure of water within the drift tube is that the analysis is very sensitive to temperature. A strong temperature correction is also derived. In order to demonstrate that the approach is reasonable, the relevant ion chemistry was measured.

2. Experimental

2.1. PTR-MS general description

The PTR-MS used in this study is one of the first instruments commercially produced by IONICON. Detailed descriptions of the operational principles of the PTR-MS and its applications are available in several review articles [14,21]. The PTR-MS instrument consists of a hollow cathode ion source, a drift tube reaction region, a quadrupole mass spectrometer, and an ion detector.

H_3O^+ reagent ions are created by ionization of water vapor within a hollow cathode ion source. Most of the water vapor from the hollow cathode is removed by a turbo molecular pump, however, a small amount diffuses into the drift tube. The magnitude of the reagent ion signals is dependent on the water flow rate to the hollow cathode, the voltages applied to the ion source extraction lenses, and the intensity of the electric field applied to the drift tube. It should be noted that because the hollow cathode ion source operates at a lower pressure than the drift tube, a small amount of the sampled ambient air enters the ion source region leading to a small (1–2% of total H_3O^+ reagent ion intensity), but unwanted production of O_2^+ ions, since O_2^+ reacts with H_2O only slowly by clustering.

The drift tube is formed from a series of resistively coupled stainless steel rings separated by Viton o-rings. The drift tube is not temperature controlled and operates at ambient temperature, which varied from 292 to 308 K during this study period. The sample enters the drift tube via a pressure-controlled inlet [22] from which a small portion of the flow (~20 standard cm^3 min^{-1}) enters the drift tube through a small section of restrictive Teflon capillary. During this study, the average drift tube pressure was 2.05 mbar. The voltage applied to the drift tube was 600 V which translates into an effective field energy expressed as the electric field strength divided by the gas number density (E/N) of 125–132 Td (1 Td = 10^{-17} V cm^2 molecule^{-1}). The variation in the E/N ratio occurs as a result of the changes in the gas number density with temperature. The magnitude of the E/N is important because it controls the extent of hydration of the H_3O^+ reagent ions and the transport time (reaction time) of the reagent ions through the drift tube. The $H_3O^+(H_2O)_n$ reagent ions drift through the ambient sample under the influence of an electric field, and undergo proton transfer reactions with any component having a proton affinity greater than that of water. A small fraction of the reagent ions and resulting product ions are sampled through a small orifice at the end of the drift tube.

Ions exiting the drift tube are focused into a quadrupole mass spectrometer where they are mass analyzed and detected using a secondary electron multiplier operated in the pulse counting mode.

The intensities of the primary reagent ions H_3O^+ and $H_3O^+(H_2O)$ are typically too large to measure directly and are determined by monitoring minor O-18 isomeric forms at m/z 21 and m/z 39, where no other ions occur in comparable abundance. The actual ion intensities are obtained by first correcting the measured ion intensities for transmission bias followed by correction for the isotopic dilution where $I_{H_3O^+} = I_{m/z\,21} \times 500$ and $I_{H_3O^+\,H_2O} = I_{m/z\,39} \times 250$. The expression that relates substrate concentration $[R]$ to the appropriately corrected ion intensities is provided below in its linear form, which is valid when the extent of reaction is small.

$$[R] = \frac{I_{RH^+}}{kt(I_{H_3O^+} + X \times I_{H_3O^+H_2O})} \frac{1}{N_{tot}} \quad (1)$$

where I_{RH^+} is the transmission corrected ion intensity of the protonated product molecule (m/z 28 for $HCNH^+$), k is the proton transfer reaction rate coefficient, t is the reaction time, X is a scaling factor that accounts for any difference in the reactivity of $H_3O^+(H_2O)$ relative to H_3O^+ and N_{tot} is the total gas number density within the drift tube. In the present study, any concentrations computed using Eq. (1) employ $k = 2 \times 10^{-9}$ cm^3 molecule^{-1} s^{-1} and $X = 1$. These assumptions are for simplicity and are discussed later in the manuscript.

2.2. Calibration experiments

Multipoint calibration experiments were performed under a variety of humidity conditions designed to span the range of typical operational conditions of the PTR-MS. Different sample humidity conditions were created through changes in the ion source water flow and the humidity level of the dilution gas. Dilution gases included dry compressed air, hydrocarbon free room air, and hydrocarbon free humidified room air. Hydrocarbon free air was generated by passing either the ambient or the humidified air streams through a heated (~400 °C) Pt catalyst (Shimadzu), which removes any oxidizable impurities from the gas stream. Humidified air was generated by allowing air to equilibrate with room temperature water within a 1-L flask. Headspace from the flask was then directed to the calibration system. Small perturbations in the humidity of the dilution gas prepared in this way due to fluctuations in the temperature of water certainly occur. These variations, along with the change in humidity that occurs when the dilution gas is mixed with a dry HCN standard, increase the uncertainty of the calibration experiments. Changes in humidity resulting from dilution were maintained at less than 10%. Dry compressed air (General Distributing) was treated to remove any residual water or hydrocarbon impurities using a water trap and the heated catalyst. Variable HCN concentrations were prepared by dynamic dilution of the HCN gas standard with one of the dilution gases. The mass flow of the HCN gas standard was held constant at 5 standard cm^3 min^{-1} (MKS 20 standard cm^3 min^{-1} mass flow controller) and the dilution flows were varied from 60 to 300 standard cm^3 min^{-1} using a 1000 standard cm^3 min^{-1} (MKS) mass flow controller. Fig. 1 shows a typical 4-point calibration curve where the right axis shows the measured (uncorrected for transmission bias) ion intensity of the m/z 28 ($HCNH^+$) signal versus the delivered HCN concentration. The left axis shows the computed HCN concentration using Eq. (1) where the slope of the line represents the detection efficiency.

A certified HCN gas standard (Matheson) with a stated concentration of 1.1 ppmv in N_2 was purchased specifically for this project and was used as delivered. However, the detection efficiencies were considerably lower (~ a factor of 3) than those previously reported [10,12,13] which led us to question the stated concentration of the standard. Therefore, the standard was analyzed by FTIR at the United States Department of Agriculture (USDA) Fire Sciences Laboratory in Missoula, Montana. That analysis indicated

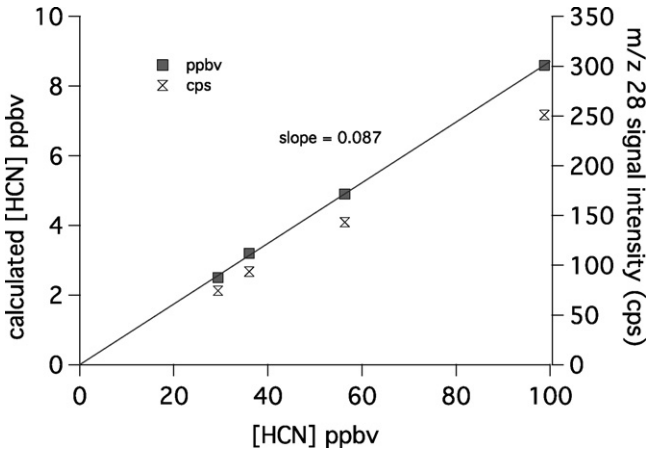

Fig. 1. HCN calibration curve. The right hand axis shows the actual measured ion signal (uncorrected for ion transmission) as a function of concentration. The left hand axis shows the HCN concentration computed via Eq. (9). The slope represents the detection efficiency.

that the HCN concentration was only 0.4 ppmv. The concentration was determined by comparing the area under the Q-branch peak centered at 712.3 cm^{-1} in the absorbance spectrum of our standard to the peak area calculated from two different reference spectra. We assume that the USDA analysis is correct and that the HCN concentration in the standard was 0.4 ppmv.

2.3. Kinetics

Relevant HCN ion chemistry kinetic processes were characterized in a selected ion flow tube (SIFT) that has been described thoroughly in previous publications [23–25], so only a few details are given here. Ions were made by electron impact in a moderate pressure source gas. $H_3O^+(H_2O)_n$ ions were made from water vapor generated from an evacuated room temperature distilled H_2O sample. H_3O^+ was injected directly. $H_3O^+(H_2O)$ (90% pure) was formed from $H_3O^+(H_2O)_2$ injection. In order to study $H_3O^+(H_2O)_2$ reactions, it was necessary to use deuterium substitution to avoid a mass coincidence with $H_2CN^+(HCN)$, which is a secondary product ion of the observed chemistry. To avoid complete declustering of the second hydrate ($n = 2$), an H_2 buffer (AGA, 99.999%) was used instead of the usual He buffer (AGA, 99.995%). Partial isotopic substitution with D_2O occurred, leading to a distribution of isomers. Rate constants were measured for $H_5D_2O_3^+$ only, since breakup was still a problem and this was a minor species. HCN was introduced as a 10% mixture in He (Matheson). H_2CN^+ ions were made in the ion source using this mixture and $H^+(HCN)(H_2O)$ was made by adding a combination of this gas mixture and H_2O to the source. In order to get even small signals of this ion, the upstream quadrupole was operated in an RF only mode, precluding mass selection. Therefore, product information could not be obtained for reactions with this ion. Rate constants with this technique are accurate to ±25% [23–25].

2.4. Ambient measurements

The PTR-MS was installed on-board the Aerodyne Mobile Laboratory (AML) [26] in October 2007 for the purpose of collecting data on the ambient atmosphere. The measurement period spanned 13 days from October 24th to November 5th 2007. During this time the AML was parked adjacent to the Aerodyne facility, which is located in a technical park about 20 miles northwest of Boston. A major highway that serves as a commuter route and experiences high traffic volumes during the morning and evening rush hours lies approximately 140 m to the southwest of the deployment site.

Table 1
Rate constants for reactions of HCN and H_2O with various ions. Accuracy is ±25%.

Reaction	Products	Total rate constant (cm^3 $molecule^{-1}$ s^{-1})
$H_3O^+ + HCN$	$H_2CN^+ + H_2O$	3.3×10^{-9}
$H_3O^+(H_2O) + HCN$	$H^+(H_2O)(HCN) + H_2O$	2.1×10^{-9}
$H_3O^+(H_2O)_2 + HCN$	$H^+(H_2O)_2(HCN) + H_2O$	1.4×10^{-9}
$H_2CN^+ + H_2O$	$H_3O^+ + HCN$	1.5×10^{-11}
$H_2CN^+ + H_2O + He$	$H^+(H_2O)(HCN) + He$	
$H^+(H_2O)(HCN)$	$H_3O^+(H_2O) + HCN$	8.5×10^{-11}

Ambient samples were drawn into the AML via a sample line consisting of stainless steel and PFA Teflon lines using a dry scroll pump at 10 l min^{-1}. All the instruments subsampled from the main inlet line through 0.45-μm pore diameter Teflon filters to eliminate particles. Carbon monoxide (CO) was measured by a pulsed quantum cascade tunable infrared laser differential absorption spectrometer (QC-TILDAS) instrument [27]. This instrument uses a multipass cell and records the transmission spectrum over a narrow wavelength region (<1-cm^{-1}) at a high sweep rate (>3 kHz). The CO concentration is determined by fitting the measured rotational–vibrational transmission spectrum to a Voigt line shape model using the line strengths and energies from the HITRAN database [28]. The PTR-MS sampled from the main inlet through a short piece of 1/8 in. OD Teflon tubing via a pressure-controlled inlet through which the volumetric flow rate was approximately 500 cm^3 min^{-1}. The PTR-MS was operated in multiple ion detection mode and was programmed to monitor 17 ion masses at 1 s per mass plus drift tube temperature and pressure. The intensity of the O_2^+ ion was not monitored during the study period, however measurements before and after the study indicated that O_2^+ was approximately 2% of the total (H_3O^+ and $H_3O^+H_2O$) reagent ion intensity. HCN is detected at its molecular weight plus one (m/z 28). Each measurement cycle takes about 18 s. The PTR-MS was programmed to collect 60 cycles of ambient data followed by six cycles of background data and was repeated continuously over the measurement period. The entire data collection procedure was automated including the switching of solenoid valves between ambient and background modes. The instrumental background is evaluated by diverting the flow through a heated Pt catalyst. The measured concentration is determined from the difference between the ambient signal intensity and instrument background.

3. Results

3.1. Kinetics measurements

Since understanding the ion-molecule kinetics is the foundation for CIMS measurements, those results are presented first. Few measurements of the ion chemistry involved in PTR measurements of HCN have been made and none have been done recently. Here, we report measurements of the kinetics for a number of the reactions involved. As the chemistry could not be studied under the exact same conditions as used in a PTR in our selected ion flow tube, we have instead focused on the most important reactions and confined ourselves to thermally equilibrated room temperature measurements only. The results are listed in Table 1.

For the most part, the chemistry for HCN detection in a PTR begins with either proton transfer from H_3O^+ to HCN

$$H_3O^+ + HCN \rightarrow H_2CN^+ + H_2O \quad (2)$$

or ligand exchange with hydrated hydronium ion,

$$H_3O^+(H_2O) + HCN \rightarrow H^+(H_2O)(HCN) + H_2O \quad (3)$$

For reaction (2), excellent agreement is found between the present value of the rate constant of 3.3×10^{-9} cm^3 $molecule^{-1}$ s^{-1} and three previous measurements with values of 3.5, 3.5, and 4.5×10^{-9} cm^3 $molecule^{-1}$ s^{-1} [29–31]. Errors for the other measurements are approximately 25% as they rely on the fast flow technique as well. The present value is 75% of the Su-Chesnavich collision rate constant [32]. Fast kinetics is expected for exothermic proton transfer reactions [33,34]. However, a rate constant somewhat smaller than the collisional value may be expected for a reaction that is only slightly exothermic. For a fast exothermic proton transfer reaction, little kinetic energy dependence is expected and the rate constant in a PTR will probably be similar to the collision rate constant [35].

Reaction (3) is essentially thermoneutral (2.5 kJ mol^{-1} endothermic, well within the experimental uncertainty) [36] and the measured rate constant is 2.1×10^{-9} cm^3 $molecule^{-1}$ s^{-1}. That value is about half of the collision rate constant [32]. Ligand exchange reactions are often rapid when the chemistry is energetically allowed [33,34]. Previously, a rate constant of 1×10^{-10} cm^3 $molecule^{-1}$ s^{-1} was measured in a flowing afterglow [37]. In that experiment, an appreciable quantity of H_2O was inevitably present. Therefore, the slightly exothermic reverse reaction would also occur as confirmed in this study. While these are the two most prevalent primary ions in a PTR, under wet conditions the second hydrate, $H_3O^+(H_2O)_2$, is also important. We could only measure the rate constant for this ion, but the energetics indicate that it proceeds by the following slightly exothermic channel [36].

$$H_3O^+(H_2O)_2 + HCN \rightarrow H^+(H_2O)_2(HCN) + H_2O \quad (4)$$

Our experimental rate constant of 1.4×10^{-9} cm^3 $molecule^{-1}$ s^{-1} is ~40% of the collisional value [32]. Thus, all three primary proton hydrates found in a PTR react rapidly with HCN. Since they are all fast, only weak kinetic energy dependences are expected.

Subsequent reactions of the ionic species containing HCN produced by the above reactions with H_2O are thermoneutral or slightly endothermic; thus, they will be important. The reverse of reaction (2),

$$H_2CN^+ + H_2O \rightarrow H_3O^+ + HCN \quad (-2)$$

was found to be accompanied by a clustering channel,

$$H_2CN^+ + H_2O + He \rightarrow H^+(H_2O)(HCN) + He \quad (5)$$

The overall rate constant was found to be 1.5×10^{-11} cm^3 $molecule^{-1}$ s^{-1}, which is substantially larger than the previous measurement of 8.8×10^{-13} cm^3 $molecule^{-1}$ s^{-1} obtained in a flowing afterglow [37]. That value has been determined using the rate constant for reaction (2) and the equilibrium constants, which would not include the clustering component. However, we have found that the clustering channel accounted for only 10–15% of the reactivity, which cannot easily explain the difference. The energetics favor the earlier lower value, but adjusting the Gibbs free energy by 8 kJ mol^{-1} in the van't Hoff equation gives an equilibrium constant that accommodates the current value. This difference is within the uncertainty limit of the known energetics. The endothermic nature of the main channel should make reverse reaction (-2) increase substantially with increasing kinetic energy and/or temperature.

The last reaction studied was the mixed cluster reacting with H_2O,

$$H^+(H_2O)(HCN) + H_2O \rightarrow H_3O^+(H_2O) + HCN \quad (-3)$$

We measured a rate constant of 8.5×10^{-11} cm^3 $molecule^{-1}$ s^{-1} for reaction (-3). Unfortunately, the products can be identified only by using the energetics because we cannot cleanly inject the ion into the flow tube. As mentioned above, this reaction is essentially thermoneutral. Thus, this reaction will be important in a PTR because $[H_2O] \gg [HCN]$.

The subset of reactions studied here shows that the chemistry is quite extensive, which makes detailed predictions of the sensitivity for HCN detection in a PTR very difficult, especially considering the unknown energy dependences. In addition, various clustering reactions and quasi-thermal (by drift tube energy) dissociations must also be included. It is clear that not only are reactions that produce HCN-containing ions rapid, but the reactions that reconvert them back into protonated water clusters are also rapid, especially considering the large H_2O concentration. Therefore, in the following we take the practical approach of calibrating the temperature and water dependence of HCN sensitivity in a PTR rather than attempt to derive the dependences from first principles; the measured chemistry is consistent with the approach.

3.2. Ab initio calculations

The thermochemistry of some of the important reactions has been determined theoretically via geometry optimizations using *Gaussian 03* [38] at the G3 level of theory [39] for H_3O^+, H_2O, H_2CN^+, HCN and H_3O^+(HCN) to assess the literature thermochemistry for reaction (5), reaction (2) [36], and the proton affinity of HCN [15]. G3 calculations have been shown to provide reliable theoretical estimates of heats of formation with average absolute deviations of $\pm 4\,kJ\,mol^{-1}$. For a direct comparison with the values of Meot-ner and Speller [36], the enthalpy of reaction at 298 K has been calculated for reactions (5) and (2) using the G3 theoretical 298 K enthalpies. These results are summarized in Table 2. The clustering reaction (5) has a calculated enthalpy of $120 \pm 6\,kJ\,mol^{-1}$, which agrees within the uncertainties, with the literature value of $115 \pm 6\,kJ\,mol^{-1}$. The proton transfer reaction (2) has a G3 enthalpy of reaction of $-24 \pm 6\,kJ\,mol^{-1}$, which is again in reasonable agreement with the $-21 \pm 4\,kJ\,mol^{-1}$ of Meot-ner and Speller [36]. The proton affinity of HCN at the G3 level of theory is $707\,kJ\,mol^{-1}$, which is in excellent agreement with the average literature value of $712\,kJ\,mol^{-1}$ determined at different levels of theory [40,41]. Consequently, the energetics in the literature can be used to analyze the observed kinetics; however, adjustments to the values of $\pm 6\,kJ\,mol^{-1}$ are not unreasonable considering the uncertainties in their determinations.

3.3. PTR-MS calibration

It is clear from the above discussion that HCN can be detected in a PTR instrument, but the chemistry is too complicated to predict the sensitivity simply based on first principles. Obviously, the sensitivity for HCN will be lower than for molecules without back reactions involving H_2O. Therefore, a comprehensive calibration procedure is needed. In particular, both temperature and water concentration dependences need to be addressed. In this section, such a calibration procedure is outlined. It relies on the $H_3O^+(H_2O)_n$ distribution as a surrogate for a true $[H_2O]$ measurement. It will be seen that this procedure provides an excellent representation of the calibration data.

We start the derivation by assuming that H_3O^+ is the only primary ion. This assumption is clearly not valid, but has been made to keep the resulting expressions simple for the purpose of discussion. Since the concentration of water is always much greater than the concentration of HCN then $k_{-2}[H_2O] \gg k_2[HCN]$ and the H_2CN^+ concentration can be given as:

$$[H_2CN^+] = \frac{k_2[HCN][H_3O^+]}{k_{-2}[H_2O]}(1 - e^{-k_{-2}t[H_2O]}) \quad (6)$$

Solving Eq. (6) for the [HCN] then substituting measured ion intensities for the ion concentrations yields Eq. (7):

$$[HCN]_o = \frac{I_{H_2CN^+}k_{-2}[H_2O]}{I_{H_3O^+}k_2(1 - e^{-k_{-2}t[H_2O]})} \quad (7)$$

The substitution of ion intensities for concentrations is permitted because only the ion concentration ratios are needed. Any potential mass discrimination is accounted for by the use of transmission corrected ion intensities. While this equation is a simplification of the actual chemistry, it does show that strong dependences on both the H_2O concentration and temperature arise, the latter of which occurs mainly via k_{-2}. The water concentration $[H_2O]$, is related to the ratio of $H_3O^+(H_2O)$ to H_3O^+ by the equilibrium constant for the clustering reaction of H_2O to H_3O^+:

$$H_3O^+ + H_2O \overset{K_{eq}}{\rightleftharpoons} H_3O^+(H_2O) \quad (8)$$

The equilibrium is strongly dependent on temperature and the E/N.

We note that in the limit of negligible concentrations of H_2O, Eq. (7) simplifies to the traditional PTR equation:

$$[HCN] = \frac{I_{H_2CN^+}}{k_2 t \cdot I_{H_3O^+}} \quad (9)$$

The detection efficiency, i.e., the ratio of the concentration computed ignoring the effect of water to the actual concentration, can then be described by $[HCN]/[HCN]_o$. Combining Eqs. (7) and (9) gives the detection efficiency:

$$\frac{[HCN]}{[HCN]_o} = \frac{1 - e^{-k_{-2}t[H_2O]}}{k_{-2}t[H_2O]} \quad (10)$$

$[H_2O]$ is related to the equilibrium constant for reaction (8):

$$[H_2O] = \frac{I_{H_3O^+H_2O}}{K_{eq}I_{H_3O^+}} \quad (11)$$

After substituting the known enthalpy into K_{eq} above and assuming k_{-2} has an Arrhenius form where the activation energy equals the endothermicity, Eq. (11) can be used in Eq. (10) to obtain,

$$\frac{[HCN]}{[HCN]_o} = \frac{I_{H_3O^+}(1 - e^{-k_{-1}t[H_2O]})C_1 \exp(+156\,kJ\,mol^{-1}/RT_{eff})}{I_{H_3O^+H_2O}} \quad (12)$$

where C_1 is related to the entropy term in K_{eq} divided by the pre-exponential factor for k_{-2} and T_{eff} is related to both the temperature and the kinetic energy of the ions in the drift tube. This approach has been chosen because it clearly illustrates how the detection efficiency is reduced in the presence of H_2O. It may be possible to derive a more complex expression based on the complete chemistry and to estimate all temperature dependences, but it is shown below that it is not necessary in order to obtain an accurate calibration. Additionally, T_{eff} is hard to calculate from first principles for complex chemistry. Nevertheless, Eq. (12) shows that a steep temperature dependence is expected.

As values for a number of the variables in Eq. (12) are not explicitly known, a series of calibration experiments have been conducted over a wide range of humidities within a relatively narrow,

Table 2
Summary of the calculated and measured reaction enthalpies for reactions (2) and (5).

Reaction	Products	ΔH_{rxn} G3 ($kJ\,mol^{-1}$)	ΔH_{rxn}[a] Lit. ($kJ\,mol^{-1}$)
$H_3O^+ + HCN$	$H_2CN^+ + H_2O$	−24	−21
$H_2CN^+ + H_2O + He$	$H^+(H_2O)(HCN) + He$	−120	−115

[a] Meot-ner and Sellers [36].

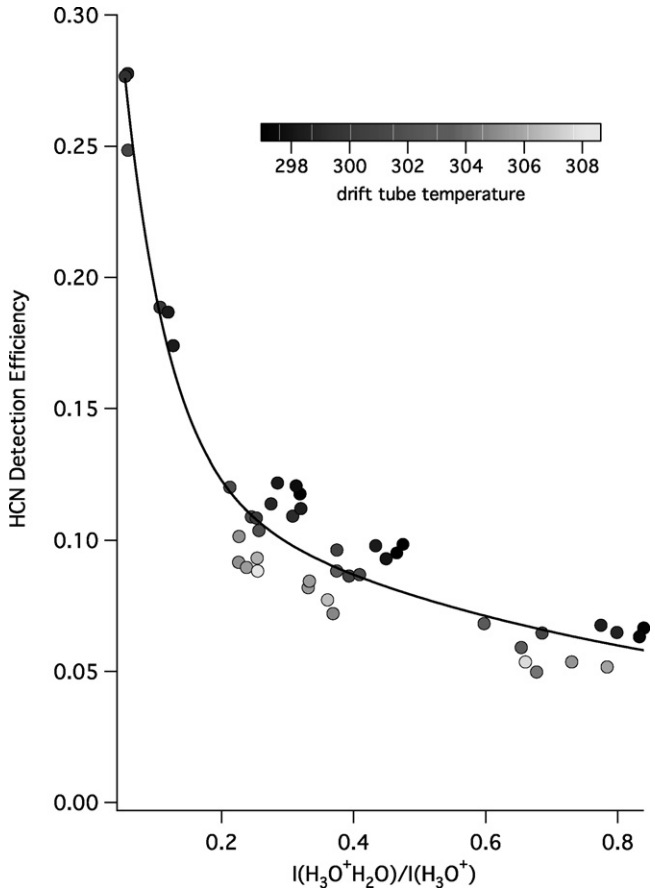

Fig. 2. Influence of water vapor concentration expressed as the ratio of reagent ion cluster distribution on the detection of HCN.

but important, range of temperature. Fig. 2 shows the observed detection efficiency (determined from the slopes of calibration experiments such as that shown in Fig. 1) plotted against the measured $H_3O^+(H_2O)$ to H_3O^+ ion intensity ratio, which is the surrogate measurement for the concentration of water. The data points have been colored to reflect the different temperature conditions. This figure clearly demonstrates that the detection efficiency decreases as the $[H_2O]$ increases, primarily through the increased importance of reverse reaction (-2) and, to a lesser extent, through the reduced rate constants for reactions (3) and (4). The sensitivity of the reagent ion clustering equilibrium reaction (8) to changes in $[H_2O]$, as well as the influence of the reaction temperature, is clearly seen in Fig. 2. It is important to reiterate that the absolute value of detection efficiencies reported in Fig. 2 are based on our initial assumption that a single reaction rate coefficient of 2×10^{-9} cm^3 molecule^{-1} s^{-1} can be used to describe the reactivity of both H_3O^+ and $H_3O^+H_2O$ reagent ions species. If larger reaction rate coefficients are employed this will shift the detection efficiency downwards while the detection efficiency would shift upwards if smaller reaction rate coefficients are used. Beyond the determination of the actual detection efficiency, the exact value of the reaction rate coefficient used is not important since the calibration procedure inherently accounts for this. What should be important is whether the H_3O^+ and $H_3O^+H_2O$ ions react at different rates. The SIFT experiments indicate that proton transfer from $H_3O^+H_2O$ is about 64% as efficient as H_3O^+, which suggests that a value of $X = 0.64$ should be used in Eq. (1). Even though the value of X should be important no observable improvement in the scatter of data occurred when X was varied from 0.5 to 1. As a result, the initially assumed value of $X = 1$ was retained in all the calculations.

The results shown in Fig. 2 can be directly compared to several other PTR-MS evaluations of the HCN response since these other studies also assumed a reaction rate coefficient of 2×10^{-9} cm^3 molecule^{-1} s^{-1}. Karl et al. [13] compared the concentrations derived from their PTR-MS measurements to those obtained using FTIR. They found that PTR-MS concentrations were about 5 times lower (detection efficiency = 0.2) than the FTIR results. Jobson et al. [12] report sensitivity factors derived from HCN calibration experiments as a function of sample humidity and also find a significant humidity dependence. Similar to our results, they observe low detection efficiencies, even under their driest conditions. This confirms our choice of the equation with the back reaction being dominant. At 0% relative humidity, they report a sensitivity factor of about 2.8 ncps/ppbv (normalized counts per second per ppbv) for HCN, while other compounds like methanol and acetonitrile ranged from 15 to 35 ncps/ppbv. These results imply that their detection efficiency under dry conditions is probably somewhere between 0.08 and 0.2, which is similar to the 0.18 result observed here with dry air and a small water flow through the hollow cathode ion source. At their highest humidity level (80% RH), the sensitivity factor for HCN dropped to about 1 ncps/ppbv, indicating a detection sensitivity in the range of 0.03–0.07, which is comparable with the data shown in Fig. 2. Qualitatively the results reported here and that of Karl et al. [13] and Jobson et al. [12] are self consistent to the extent to which direct comparisons can be made because of differences in drift tube temperature, hollow cathode ion source water flow and sample humidity.

As previously stated, the goal of this study was to develop an empirical relationship between the HCN detection efficiency and the parameters routinely measured in a PTR-MS such as $H_3O^+(H_2O)$ and H_3O^+ ion ratios and temperature. As a start, we substitute the concentration of water described in Eq. (11) into Eq. (10). The x-axis variable then becomes $(1 - e^{(-k_{-2}tI_{(H_3O^+H_2O)}/K_{eq}I_{H_3O^+})})/(k_{-2}tI_{(H_3O^+H_2O)}/K_{eq}I_{H_3O^+})$, where the effective back reaction rate constant, k_{-2}, and K_{eq} (see Table 3 – through the effective temperature) are used as fitting variables. Effective temperature defines the magnitude of K_{eq} that is used to represent the concentration of water in the drift tube in conjunction with observed proton hydrate cluster ion distribution via Eq. (11). Fig. 3 shows the calibration data plotted versus this variable. The best fit is found using $k_{-2} = 2 \times 10^{-11}$ cm^3 molecule^{-1} s^{-1} and an effective temperature of $(474\,K + T_{drift})$, where T_{drift} is the measured drift tube temperature. While the plot in Fig. 3 is reasonably linear, we note that a temperature dependence in the detection efficiency still remains. We also note that the intercept is non-zero.

Figs. 2 and 3 clearly indicate the sensitivity of results with respect to temperature. Temperature exerts an influence on the

Table 3
Best-fit parameters determined for the HCN detection efficiency via Eq. (13).

Fitting parameter	Value		
k_{-1}	2×10^{-11} cm^3 molecule^{-1} s^{-1}		
t	1×10^{-4} s		
[a] K_{eq}	$\Delta H = -132$ kJ mol^{-1}	$\Delta S = 100$ J K^{-1} mol^{-1}	$T = 474\,K + T_{drift}$
n	10		

[a] $K_{eq} = \exp^{-(\Delta G/RT)}$ where $\Delta G = \Delta H - T\Delta S$ Thermodynamic values are taken from [47].

results not only directly through the normal temperature dependent phenomena (buffer gas number density and the magnitude of endothermic reaction rate coefficients), but also indirectly through changes in the field energy variable E/N. For instance the reaction time is directly dependent on E/N but is also influenced the distribution of $H_3O^+(H_2O)_n$ reagent ions through their reduced mobilties. The position of the equilibrium reaction, Eq. (9), and magnitude of $HCNH^+ + H_2O$ reaction rate constant, Eq. (-2), are also dependent on both temperature and E/N. Another difficulty is that there is evidence that a fraction of the $H_3O^+(H_2O)$ ions undergo dissociative collisions within the expansion region between the drift tube and the entrance aperture to the mass spectrometer. Thus, they are detected as H_3O^+. This phenomenon is also likely to depend on both temperature and E/N. To deal with the complexity of all of the temperature and E/N dependent variables, requires adding another adjustable temperature dependent term to our expression. To accomplish this, we have chosen a power law form proportional to the number density $(P_1T_2/P_2T_1)^n$, where P_2 (2.048 mbar) and T_2 (302.5 K) are midpoint experimental pressures and temperatures and P_1 and T_1 are the actual recorded experimental temperatures. Our final calibration expression is then,

$$\frac{[HCN]_0}{[HCN]} = \frac{1 - e^{-k_{-1}t[H_2O]}}{k_{-1}t[H_2O]} \left(\frac{P_1T_2}{P_2T_1}\right)^n \quad (13)$$

where $[H_2O]$ is computed from the measured H_3O^+ and $H_3O^+(H_2O)$ ion intensities via Eq. (11) and the parameters listed in Table 3 for the determination of K_{eq}. The power, n, subsequently becomes an additional fitting parameter. The results of adding this additional fitting parameter are shown in Fig. 4, where $n = 10$. Inspection of Fig. 4 illustrates that Eq. (13) effectively accounts for the observed

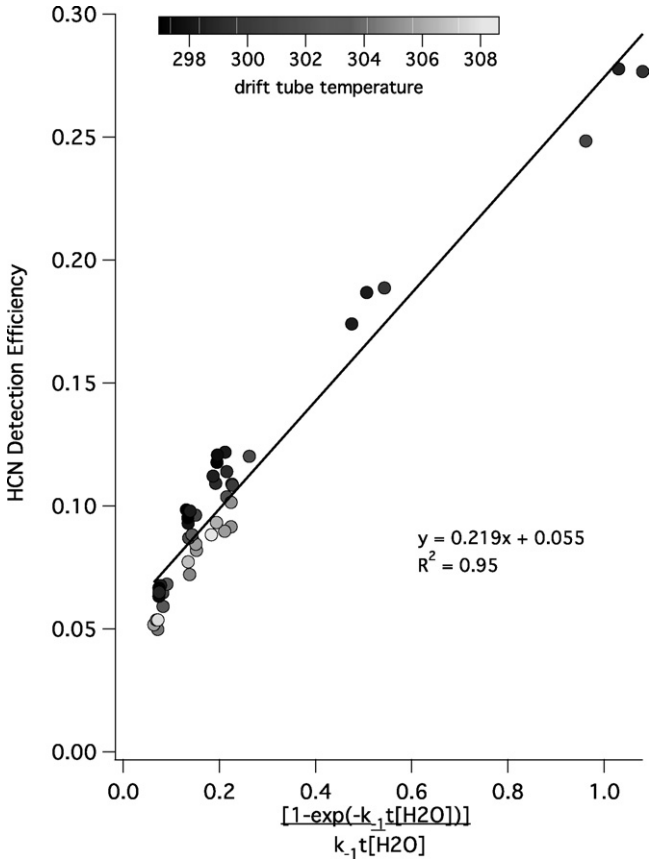

Fig. 3. Best fit of the HCN detection efficiency to the expression given in Eq. (10). $[H_2O]$ is calculated from Eq. (11) from the parameters listed in Table 3 and the measured H_3O^+ and $H_3O^+(H_2O)$ intensities.

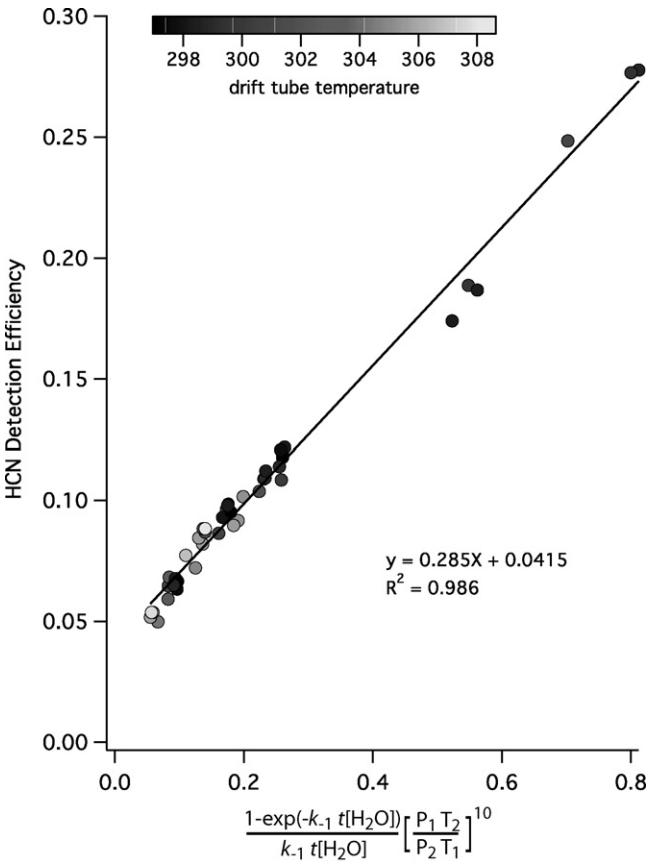

Fig. 4. Best fit of the HCN detection efficiency to the expression given in Eq. (13). $[H_2O]$ is calculated from Eq. (11) from the parameters listed in Table 3 and the measured H_3O^+ and $H_3O^+(H_2O)$.

temperature dependence over the complete set of calibrations with a maximum deviation from the best-fit line of ±12%. While we do not attempt to attach physical significance to the correction factor, the above discussion clearly shows that some type of correction is warranted and this was a convenient way of introducing one. The low scatter in Fig. 4 shows that we have achieved our desired goal of obtaining a well-defined relationship between detection efficiency and typical experimentally measured parameters.

3.4. Ambient HCN measurements

Fig. 5 shows the calculated HCN detection efficiency along with the experimental measurements of drift tube pressure, drift tube temperature and the $H_3O^+H_2O$ to H_3O^+ ion intensity ratio for the 13-day measurement period. The HCN detection efficiency was computed using the equation shown in Fig. 4, $y = 0.285x + 0.0415$ where y equals the detection efficiency and x represents the right hand side of Eq. (13). The value of x was computed using $[H_2O]$ determined via Eq. (11) in conjunction with the best-fit parameters listed in Table 3. The calculated detection efficiency varied from a low of 0.063 to a high of 0.16 with an average value of 0.082. With the exception of a single large excursion, the calculated detection efficiency typically stayed within the range of 0.07–0.10. The large change in the detection efficiency profile that occurred on October 29, 2007 was the result of a decrease in the water flow to the hollow cathode ion source. The water flow rate to the hollow cathode ion source decreased because the temperature of the water supply became too cold. Normal water flow returned the next day after the water supply returned to its previous, warmer temperature. While the calibration procedure is designed to accommodate changes in

the water flow to the hollow cathode ion source there are other consequences, which include a concomitant rise in the O_2^+ signal that impact the validity of the data collected during this period. The influence of O_2^+ on the measurement is discussed below.

PTR-MS deduced HCN concentrations corrected for the influence of water and temperature, were determined by dividing the unadjusted HCN concentration determined using Eq. (1) by the calculated detection efficiency. A time series plot of the PTR-MS deduced HCN concentration measured over the 13-day period at this suburban Boston location is shown in Fig. 6. To reduce the noise in the measurements, the 1-s data has been averaged to 18 min. Measurements of CO, a known combustion tracer, have also been included in Fig. 6. Most of the variability in HCN signal appears to be correlated with changes in CO. This correlation with CO suggests that HCN has an anthropogenic source, most likely vehicle exhaust given the close proximity of the sampling site to a major highway. However, an alternative explanation for this correlation is that there is some other compound co-emitted with CO, which is ionized and detected at the same mass-to-charge ratio as protonated HCN. Ethene has been identified as a compound that may interfere and is discussed in the next section.

3.5. Spectral interferences

While there are no known or expected spectral interferences to the detection of HCN using $H_3O^+(H_2O)_n$ reagent ions [9], ethene can interfere in PTR-MS instruments due to the unwanted formation of O_2^+ in the hollow cathode ion source. O_2^+ reacts with ethene via a charge transfer reaction to form $C_2H_4^+$ and has been used as a chemical ionization reagent ion for the detection of ethene [42]. Both $C_2H_4^+$ and $HCNH^+$ have the same nominal mass-to-charge ratio and cannot be spectrally resolved with quadrupole mass spectrometers. Even though the level of O_2^+ is only a small fraction (~2%) of the $H_3O^+(H_2O)_n$ abundance, the concentration of ethene in the ambient air impacted by anthropogenic emissions [43] is expected to be much greater than that of HCN. Because we do not have a direct measure of ethene, we have relied on emission ratios to estimate the ethene concentration. Several studies have reported ethene:CO emission ratios for the Boston area [43,44]. We have used the average of these measurements (4.5×10^{-3} mol C_2H_4/mol CO) for the present estimates. Using these derived ethene concentrations we have predicted the magnitude of response generated by the O_2^+ reaction and this result is shown as the black trace in the upper panel of Fig. 6. This calculation assumes that the intensity of O_2^+ is 2% of the total $H_3O^+(H_2O)_n$ signal and that the reaction rate constant for O_2^+ reaction with ethene is 7×10^{-10} cm^3 molecule^{-1} s^{-1} [29]. These calculations predict that 1 ppbv of ethene contributes an equivalent response to 0.1 ppbv of HCN. While the absolute interference from ethene is uncertain, the magnitude is significant enough that is needs to be considered in any PTR-MS measurement of HCN.

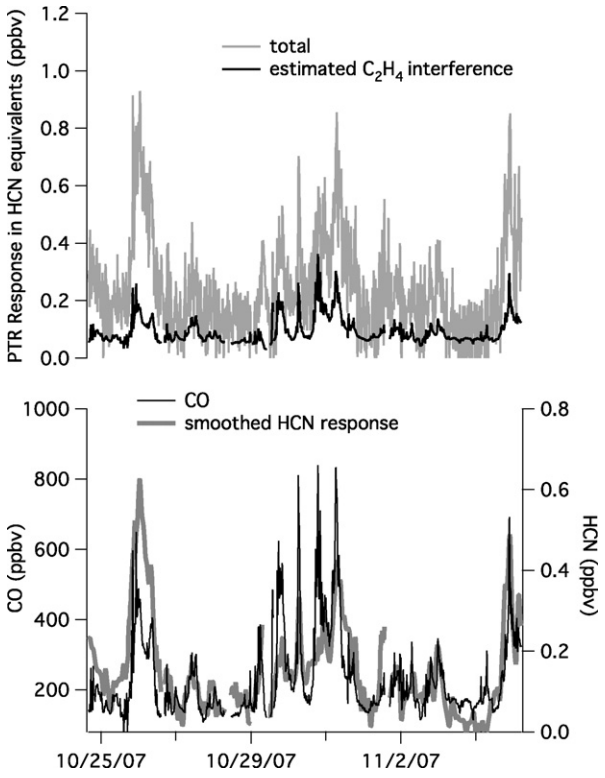

Fig. 6. PTR-MS m/z 28 response (shown as 18 min average) computed as if the total signal originates from HCN (upper panel, gray trace). The upper panel black trace shows estimated signal interference resulting from the reaction of ethene with impurity O_2^+ reagent ion (see text for discussion). The corrected HCN concentration (lower panel) was computed by subtracting the ethene signal from the total. This corrected HCN response was smoothed using a 10-point moving average and is plotted as the gray trace in the lower panel. The 18 min averaged CO data is shown as the black trace in the lower panel.

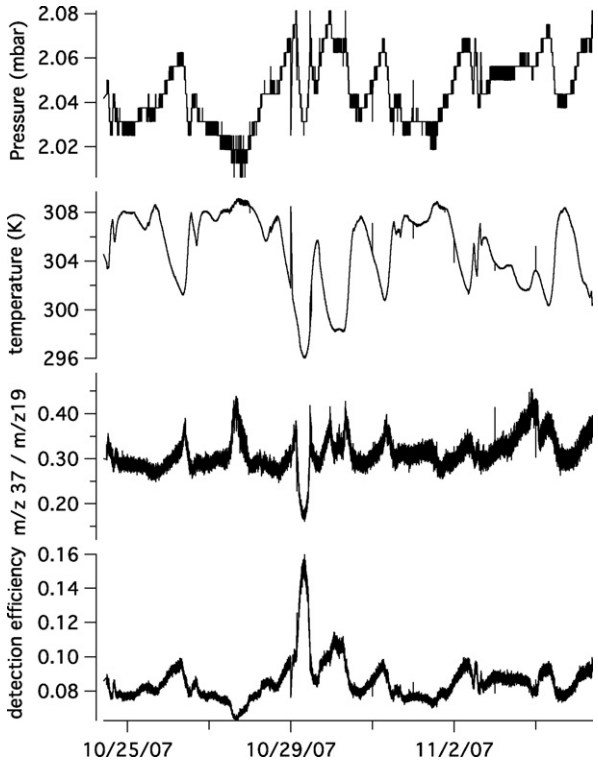

Fig. 5. Experimental parameters and the computed HCN detection efficiency measured during the ambient air-monitoring period.

3.6. Interpretation of the deduced ambient HCN concentrations

The actual HCN concentrations can be deduced from the difference between the total signal and that attributed to ethene. This result has been plotted in the lower panel of Fig. 6 where the HCN time series trace has been superimposed onto the CO measurement. Because the raw corrected signal is quite noisy, the corrected HCN signal has been smoothed using a 10-point moving average. It is immediately apparent that the smoothed HCN measurements is correlated with CO, but that HCN:CO emission ratio is not constant throughout the period. Correlation scatter plots of the corrected HCN response versus CO have been constructed and analyzed for each of the diluted road-side plumes where the CO

concentration exceeded 400 ppbv. The slopes of these plots (not shown) provide HCN:CO emission ratios. These measured HCN:CO emission ratios vary from plume to plume and span a range from 0.2 to 1.4 mmol HCN/mol CO. The variability in the emission ratios suggests that there is no simple relationship between HCN and CO. Background ambient HCN concentrations determined from the intercepts of the correlation plots or from measurements made during periods of low CO (with and without the ethene correction) appear reasonable and are in the range of the average HCN concentration (200 pptv) in the lower troposphere [1].

4. Conclusions

A comprehensive approach to PTR-MS detection of HCN is presented. The chemistry involved is complex and includes several reactions involving cluster ions. While the forward rates for proton transfer from H_3O^+ and its hydrates approach the collision limit, back reactions with the inevitable water vapor present in a PTR-MS are clearly fast enough to interfere with HCN measurements unless properly accounted for. This is because the proton affinity of HCN is only slightly greater than that of H_2O.

A detailed calibration procedure was developed to account for both water vapor and temperature dependences. In the past, PTR-MS derivations of compounds sensitive to H_2O required separate measurements of the water concentration. Here, we show that a method based on the ratio of the $H_3O^+(H_2O)$ to H_3O^+ ratio adequately accounts for the water concentration dependence. The method eliminates the need for an independent $[H_2O]$ measurement and accounts for all sources of H_2O in the drift tube reaction region. However, because both the $H_3O^+(H_2O)$ to H_3O^+ ratio and the back reaction of protonated HCN with water are sensitive to temperature, a strong temperature dependent correction is also needed, i.e., T^{-10}. This strong temperature dependence suggests that the best results will be obtained with instruments having temperature controlled drift tubes. While the exact calibration factors will be instrument dependent, this technique is broadly applicable and can be adapted for other molecules with proton affinities near to that of water, e.g., H_2CO.

The technique was used to derive ambient HCN concentrations. These measurements exhibit a background HCN value similar to those found in the lower troposphere. Measurement of HCN in the presence of ethene (i.e., automotive engine emission sources [45]) will be compromised if there is a significant O_2^+ ion signal. This is important for PTR-MS as these instruments generate a small amount of unwanted O_2^+. Accurate measurements of HCN with the PTR-MS in the presence of ethene are possible if the O_2^+ can be eliminated. One means of eliminating the O_2^+ signal would be to dope the sample with NO. O_2^+ reacts with NO to form NO^+ [29], which is unreactive towards ethene since its ionization energy is lower than that of ethene [46].

The detection of HCN using the PTR-MS technique presents significant challenges. It is recognized that if the measurement of HCN is the primary goal that other methods may be more attractive. The intent of this study was not to develop the PTR-MS technique specifically for the detection of HCN, but to provide a method that would allow for its measurement when no other technique is available. Given the diverse range of studies in which PTR-MS instruments are deployed, the ability to extract quantitative information on the concentration of HCN may help enhance our understanding of the emission sources of this important compound in our atmosphere.

Acknowledgements

We thank and acknowledge Ted Christian and Robert Yokelson at University of Montana for their assistance in validating the concentration of our HCN standard and for their help in preparing this work for publication. We gratefully acknowledge Don Hunton for his helpful discussions. A.A.V. and A.J.M. are supported by the United States Air Force of Scientific Research (AFOSR) under Project No. 2303EP4. A.J.M. is supported under contract No. FA8718-04-C-0006 to Boston College. W.B.K, S.C.H, E.C.W and C.E.K were supported by the US Department of Energy Atmospheric Sciences Program under Contract No. DE-FG02-05ER62982. W.B.K and E.C.F were supported by National Science Foundation under Grant No. 0242922.

References

[1] Q.B. Li, D.J. Jacob, R.M. Yantosca, C.L. Heald, H.B. Singh, M. Koike, Y.J. Zhao, G.W. Sachse, D.G. Streets, J. Geophys. Res. Atmos. 108 (2003) 8827, doi:10.1029/2002JD003006.
[2] C.S. Shim, Y.H. Wang, H.B. Singh, D.R. Blake, A.B. Guenther, J. Geophys. Res. Atmos. 112 (2007) D10305, doi:10.1029/2006JD007543.
[3] M.M. Baum, J.A. Moss, S.H. Pastel, G.A. Poskrebyshev, Environ. Sci. Technol. 41 (2007) 857.
[4] H.L. Karlsson, Sci. Total Environ. 334–35 (2004) 125.
[5] S. Spreng, F. Arnold, Geophys. Res. Lett. 21 (1994) 1251.
[6] A.A. Viggiano, D.E. Hunton, T.M. Miller, J.O. Ballenthin, J. Geophys. Res. Atmos. 108 (2002) 8304, doi:10.1029/2001JD001033.
[7] T.G. Custer, S. Kato, R. Fall, V.M. Bierbaum, Geophys. Res. Lett. 27 (2000) 3849.
[8] A.B. Raksit, D.K. Bohme, Can. J. Chem. 61 (1983) 1683.
[9] P. Spanel, T.S. Wang, D. Smith, Rapid Commun. Mass Spectrom. 18 (2004) 1869.
[10] T.J. Christian, B. Kleiss, R.J. Yokelson, R. Holzinger, P.J. Crutzen, W.M. Hao, T. Shirai, D.R. Blake, J. Geophys. Res. Atmos. 109 (2004) D02311, doi:10.1029/2003JD003874.
[11] R. Holzinger, C. Warneke, A. Hansel, A. Jordan, W. Lindinger, D.H. Scharffe, G. Schade, P.J. Crutzen, Geophys. Res. Lett. 26 (1999) 1161.
[12] B.T. Jobson, M.L. Alexander, G.D. Maupin, G.G. Muntean, Int. J. Mass Spectrom. 245 (2005) 78.
[13] T.G. Karl, T.J. Christian, R.J. Yokelson, P. Artaxo, W.M. Hao, A. Guenther, Atmos. Chem. Phys. 7 (2007) 5883.
[14] J. de Gouw, C. Warneke, Mass Spectrom. Rev. 26 (2007) 223.
[15] E.P. Hunter, S.G. Lias, in: P.J. Linstrom, W.G. Mallard (Eds.), NIST Chemistry WebBook, NIST Standard Reference Database Number 69, National Institute of Standards and Technology, Gaithersburg MD, accessed December 2008.
[16] A. Hansel, W. Singer, A. Wisthaler, M. Schwarzmann, W. Lindinger, Int. J. Mass Spectrom. 167 (1997) 697.
[17] S. Inomata, H. Tanimoto, S. Kameyama, U. Tsunogai, H. Irie, Y. Kanaya, Z. Wang, Atmos. Chem. Phys. 8 (2008) 273.
[18] M. Steinbacher, J. Dommen, C. Ammann, C. Spirig, A. Neftel, A.S.H. Prevot, Int. J. Mass Spectrom. 239 (2004) 117.
[19] A. Wisthaler, E.C. Apel, J. Bossmeyer, A. Hansel, W. Junkermann, R. Koppmann, R. Meier, K. Muller, S.J. Solomon, R. Steinbrecher, R. Tillmann, T. Brauers, Atmos. Chem. Phys. 8 (2008) 2189.
[20] C. Ammann, A. Brunner, C. Spirig, A. Neftel, Atmos. Chem. Phys. 6 (2006) 4643.
[21] W. Lindinger, A. Hansel, A. Jordan, Chem. Soc. Rev. 27 (1998) 347.
[22] S.C. Herndon, T. Rogers, E.J. Dunlea, J.T. Jayne, R. Miake-Lye, B. Knighton, Environ. Sci. Technol. 40 (2006) 4406.
[23] A.A. Viggiano, S.T. Arnold, R.A. Morris, Int. Rev. Phys. Chem. 17 (1998) 147.
[24] A.A. Viggiano, R.A. Morris, F. Dale, J.F. Paulson, K. Giles, D. Smith, T. Su, J. Chem. Phys. 93 (1990) 1149.
[25] A.A. Viggiano, R.A. Morris, J. Phys. Chem. 100 (1996) 19227.
[26] S.C. Herndon, J.T. Jayne, M.S. Zahniser, D.R. Worsnop, B. Knighton, E. Alwine, B.K. Lamb, M. Zavala, D.D. Nelson, J.B. McManus, J.H. Shorter, M.R. Canagaratna, T.B. Onasch, C.E. Kolb, Faraday Discuss. 130 (2005) 327.
[27] S.C. Herndon, M.S. Zahniser, D.D. Nelson, J. Shorter, J.B. McManus, R. Jimenez, C. Warneke, J.A. de Gouw, J. Geophysical Res. Atmos. 112 (2007) D10S03, doi:10.1029/2006JD007600.
[28] L.S. Rothman, D. Jacquemart, A. Barbe, D.C. Benner, M. Birk, L.R. Brown, M.R. Carleer, C. Chackerian, K. Chance, L.H. Coudert, V. Dana, V.M. Devi, J.M. Flaud, A.A. Gamache, A. Goldman, J.M. Hartmann, K.W. Jucks, A.G. Maki, J.Y. Mandin, S.T. Massie, J. Orphal, A. Perrin, C.P. Rinsland, M.A.H. Smith, J. Tennyson, R.N. Tolchenov, R.A. Toth, J. Vander Auwera, P. Varanas, G. Wagner, J. Quant. Spectrosc. Radiat. Transfer 96 (2005) 139.
[29] C.G. Freeman, P.W. Harland, J.P. Liddy, M.J. McEwan, Aust. J. Chem. 31 (1978) 963.
[30] G.I. Mackay, S.D. Tanner, A.C. Hopkinson, D.K. Bohme, Can. J. Chem. 57 (1979) 1518.
[31] G.I. Mackay, D. Betowski, J.D. Payzant, H.I. Schiff, D.K. Bohme, J. Phys. Chem. 80 (1976) 2919.
[32] T. Su, W.J. Chesnavich, J. Chem. Phys. 76 (1982) 5183.
[33] Y. Ikezoe, S. Matsuoka, M. Takebe, A.A. Viggiano, Gas Phase Ion-Molecule Reaction Rate Constants Through 1986, Maruzen Company, Ltd., Tokyo, 1987.
[34] V. Anicich, An Index of the Literature for Bimolecular Gas Phase Cation-Molecule Reaction Kinetics, Jet Propulsion Laboratory 03–19, Pasadena, CA, 2003.
[35] T. Su, J. Chem. Phys. 82 (1985) 2164.
[36] M. Meot-Ner, C.V. Speller, J. Phys. Chem. 93 (1989) 3663.
[37] K. Tanaka, G.I. Mackay, D.K. Bohme, Can. J. Chem. 56 (1978) 193.
[38] M.J. Frisch, G.W. Trucks, H.B. Schlegel, G.E. Scuseria, M.A. Robb, J.R. Cheeseman, J.A. Montgomery, T. Vreven, K.N. Kudin, J.C. Burant, J.M. Millam, S.S. Iyengar, J.

Tomasi, V. Barone, B. Mennucci, M. Cossi, G. Scalmani, N. Rega, G.A. Petersson, H. Nakatsuji, M. Hada, M. Ehara, K. Toyota, R. Fukuda, J. Hasegawa, M. Ishida, T. Nakajima, Y. Honda, O. Kitao, H. Nakai, M. Klene, X. Li, J.E. Knox, H.P. Hratchian, H.J.B. Cross, C. Adamo, J. Jaramillo, R. Gomperts, R.E. Stratmann, O. Yazyev, A.J. Austin, R. Cammi, C. Pomelli, J.W. Ochterski, P.Y. Ayala, K. Morokuma, G.A. Voth, P. Salvador, J.J. Dannenberg, V.G. Zakrzewski, S. Dapprich, A.D. Daniels, M.C. Strain, O. Farkas, D.K. Malick, A.D. Rabuck, K. Raghavachari, J.B. Foresman, J.V. Ortiz, J.Q. Cui, A.G. Baboul, S. Clifford, J. Cioslowski, B.B. Stefanov, G. Liu, A. Liashenko, P. Piskorz, I. Komaromi, R.L. Martin, D.J. Fox, T. Keith, M.A. Al-Laham, C.Y. Peng, A. Nanayakkara, M. Challacombe, P.M.W. Gill, B. Johnson, W. Chen, M.W. Wong, C. Gonzalez, J.A. Pople, Gaussian 03W, Revision C.02, Gaussian, Inc., Pittsburgh PA, 2003.

[39] L.A. Curtiss, P.C. Redfern, K. Raghavachari, V. Rassolov, J.A. Pople, J. Chem. Phys. 109 (1998) 7764.

[40] A.L.L. East, B.J. Smith, L. Radom, J. Am Chem. Soc. 119 (1997) 9014.

[41] B.J. Smith, L. Radom, J. Am. Chem. Soc. 115 (1993) 4885.

[42] K. Sovova, M. Ferus, I. Matulkova, P. Spanel, K. Dryahina, O. Dvorak, S. Civis, Mol. Phys. 106 (2008) 1205.

[43] A.K. Baker, A.J. Beyersdorf, L.A. Doezema, A. Katzenstein, S. Meinardi, I.J. Simpson, D.R. Blake, F.S. Rowland, Atmos. Environ. 42 (2008) 170.

[44] C. Warneke, S.A. McKeen, J.A. de Gouw, P.D. Goldan, W.C. Kuster, J.S. Holloway, E.J. Williams, B.M. Lerner, D.D. Parrish, M. Trainer, F.C. Fehsenfeld, S. Kato, E.L. Atlas, A. Baker, D.R. Blake, J. Geophysical Res. Atmos. 112 (2007) D10S47, doi:10.1029/2006JD007930.

[45] J.J. Schauer, M.J. Kleeman, G.R. Cass, B.R.T. Simoneit, Environ. Sci. Technol. 36 (2002) 1169.

[46] S.G. Lias, in: P.J. Linstrom, W.G. Mallard (Eds.), NIST Chemistry WebBook, NIST Standard Reference Database Number 69, National Institute of Standards and Technology, Gaithersburg MD, accessed December 2008.

[47] R.G. Keesee, A.W. Castleman, J. Phys. Chem. Ref. Data 15 (1986) 1011.